Structure in narrow planetary rings: Open questions and recent results

Luis Benet* and Olivier Merlo

Instituto de Ciencias Físicas, Universidad Nacional Autónoma de México,
Apdo. Postal 48-3, 62251 Cuernavaca, Morelos, Mexico.
* benet@fis.unam.mx

ABSTRACT

In this paper we review some open questions in the context of the structure observed in narrow planetary rings, and summarize some recent results of our work directed to answer them. Using the scattering approach to narrow rings we have succeeded to reproduce some of their structural properties in a qualitative sense, using unrealistic toy models as examples. We obtain narrow rings which are non-circular and display sharp edges. In addition, these rings may have multiple components which may entangle in a complicated dynamically evolving way forming a braided structure, or may display strongly azimuthal dependent features such as arcs. The appearance of these structural properties can be understood in terms of the underlying phase space.

Key words: narrow planetary rings, strands, arcs, scattering approach.

RESUMEN

En este artículo hacemos una revisión de algunas de las preguntas que permanecen abiertas en el contexto de la estructura observada en los anillos planetarios delgados, y resumimos algunos resultados recientes de nuestro trabajo encaminados a responderlas. Usando el enfoque de la dispersión en anillos delgados hemos reproducido algunas de sus propiedades estructurales de forma cualitativa, usando modelos de juguete irrealistas como ejemplos. Hemos obtenido anillos delgados no circulares que muestran bordes bien definidos. Además, estos anillos pueden tener componentes múltiples que se enredan de manera complicada y evolucionan dinámicamente formando estructuras trenzadas, o pueden exhibir estructuras con una fuerte dependencia azimutal como arcos. La aparición de estas estructuras se puede entender en términos del espacio fase subyacente.

Palabras clave: anillos planetarios delgados, componentes múltiples (hebras), arcos, enfoque de la dispersión.

INTRODUCTION: OBSERVATIONS

Saturn rings are, since their discovery by Galileo in 1610, one of the most puzzling and beautiful features of the Solar System. For a long time, Saturn had the special position being the "ringed planet". In 1977, the somewhat accidental discovery of Uranus rings by stellar-occultation measurements (Elliot *et al*., 1977) changed this view, and led to a renewed interest in ring systems. The main reason for this was that the Uranian rings turned to be extremely different from those of Saturn: They are narrow, opaque, sharp-edged, inclined and eccentric (Elliot and Nicholson, 1984; Esposito, 2002). To quote some figures (Murray and Dermott, 1999), the widest ring of Uranus, the ε ring, is

20–96 km wide with a nominal semi–major axis at 51,149 km; in comparison, the main rings of Saturn are a few thousand kilometers wide. The Uranian rings were the first narrow planetary rings discovered, but are not the only ones that exist. The Pioneer mission and the Voyagers uncovered other narrow ring in Saturn, the F ring, showing an amazing and puzzling structure; occultation measurements pointed the existence of rings around Neptune; Jupiter's broad rings were also discovered (see Esposito, 2002 for a detailed historical account). Figures 1-4 are photographs illustrating some examples of the variety of structure that is found.

These discoveries raised a number of new questions, most of which remain unanswered (Esposito, 2002; Sicardy, 2005). For instance, the eccentricity of the ε ring is 0.0079; Saturn's F ring has an eccentricity 0.0026. An eccentric inclined narrow ring like the ε ring is expected to circularize and spread in rather short time scales, $t_{max} \sim 10^8$ years, which is "considerably smaller than the age of the solar system" (Esposito, 2002). This estimate follows from inter–particle collisions, drag and differential precession. Therefore, an efficient confinement mechanism must maintain these structural properties of the ring over longer time scales allowing, among other, an eccentric ring (Esposito, 2002).

To explain the structural features of the Uranian rings, new models were introduced where the confinement was induced by nearby moons. Among these models we mention in particular the shepherding model introduced by Goldreich and Tremaine (1979), where two moons around the ring were proposed to bound it. The Pioneer and Voyager missions detected the shepherd moons around Saturn's F ring
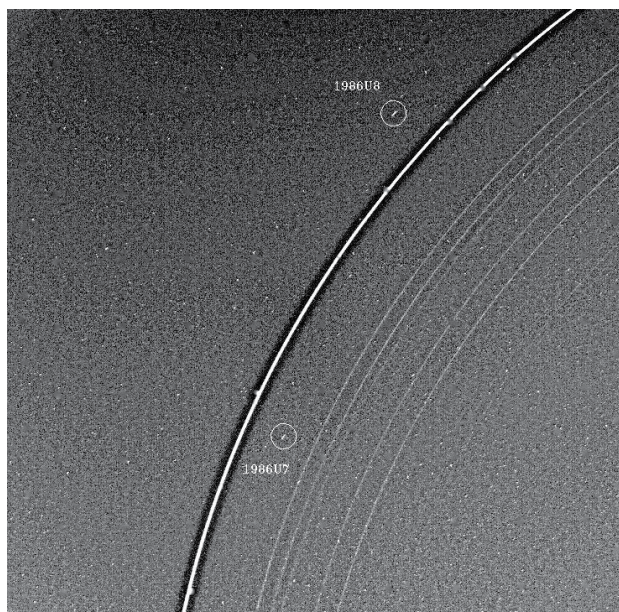
Figure 1. Uranus' rings and the "shepherd" satellites of the ε ring discovered by Voyager 2. The image was taken in January 21 of 1986 (PIA01976. Courtesy NASA/JPL/Space Science Institute-Caltech).

and around the outermost ε ring of Uranus; these discoveries represented a confirmation of the theory. The shepherding confinement involves angular momentum transfer between the shepherd moons and the ring particles, self-gravity and viscous damping due to inter-particle collisions (Borderies *et al.*, 1983). While the full scenario for shepherding has not
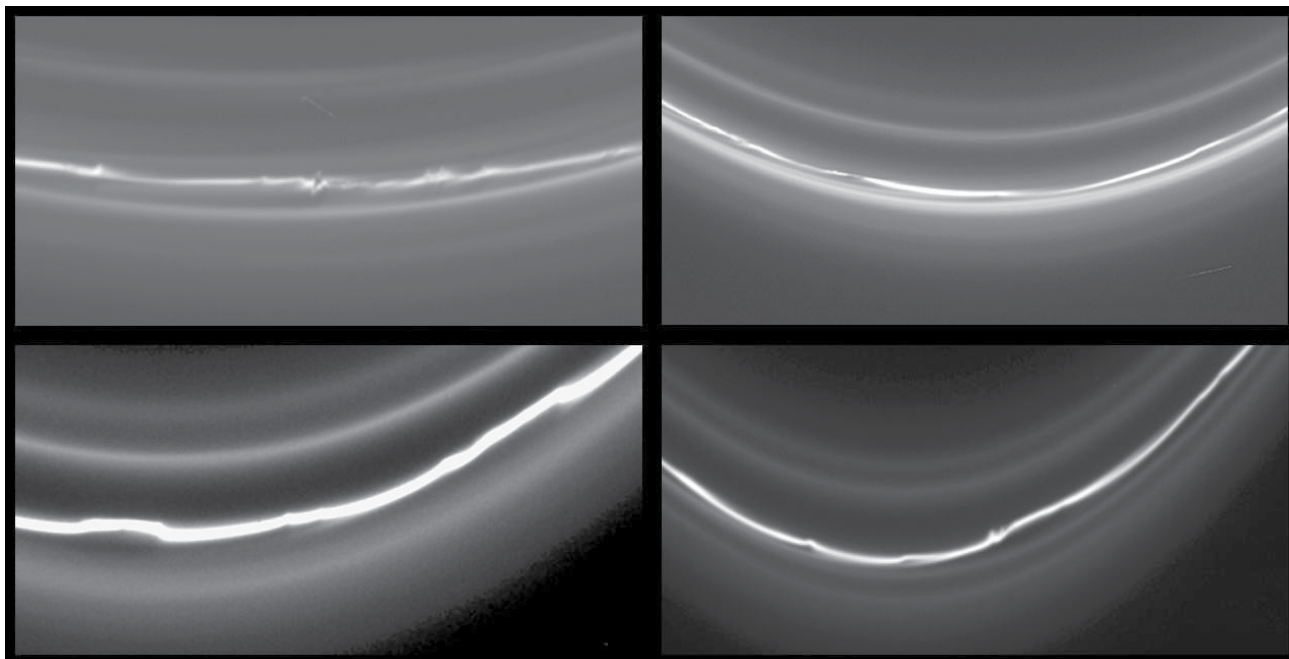
Figure 2. Structure in Saturn's F ring. These four images taken by Cassini of Saturn's F ring show the "knotted" structure in different locations. (PIA07522. Courtesy NASA/JPL/Space Science Institute-Caltech).
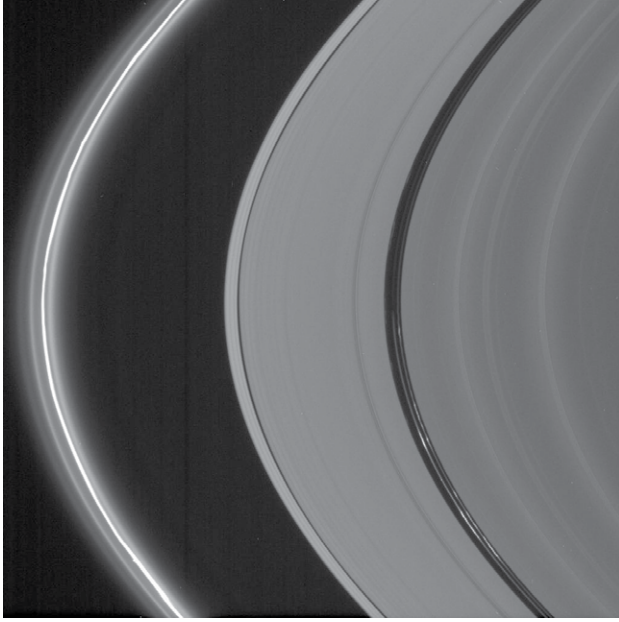
Figure 3. Ringlets in the Encke gap. (PIA08305. Courtesy NASA/JPL/ Space Science Institute-Caltech).

been fully understood (Esposito, 2002; Sicardy, 2005), the presence of dissipation seems to be essential; this is actually needed to avoid certain singularities (Ogilvie, 2007). In addition, the formulation assumes that the ring boundaries are located at a lower-order resonance.

Yet, Saturn's F ring does not fulfill the requirements to apply this theory. Moreover, most Uranian rings have no associated shepherd moons around them (Murray and Thomason, 1990), nor some narrow eccentric rings of Saturn, which among others would provide an explanation for their sharp edges (Murray and Dermott, 1999). Thus,

Figure 4. Neptune rings and Adam's arcs as seen by Voyager 2 in August of 1989. (PIA01493. Courtesy NASA/JPL/Space Science Institute-Caltech).

either the shepherds are there but are too small to be detected, or "some physics is yet to be understood" (Sicardy, 2005). Saturn's F ring turned out to have a very rich dynamical structure (Smith *et al.*, 1981; Smith *et al.,* 1982; Murray *et al.,* 1997): besides the non-zero eccentricity, it displays multiple components entangled in a complicated way, known as strands and braids, showing further puzzling features like kinks and clumps.

Numerical simulations have investigated a variety of physical interactions, like the gravitational perturbations of shepherd moons on circular and eccentric orbits (Giuliatti-Winter *et al.*, 2000; Showalter and Burns, 1982), effects due to the action of embedded moonlets (Lissauer and Peale, 1986), and ring inter-particle collision effects (Hänninen, 1993; Lewis and Stewart, 2000). The central questions investigated have been the formation of structure (strands, braids, clumps) and their short-term stability. While these studies have led to interesting predictions, *e.g.* the formation of channels and streamers (Giuliatti-Winter *et al.,* 2000) which have been recently observed by Cassini (Murray *et al.,* 2005), there is no self-consistent approach for the confinement of narrow rings and their radial and azimuthal structure. The F Saturn ring remains as the most fascinating and puzzling case.

The present paper reviews some of our recent work on this point, namely, a self-consistent scenario for the occurrence of narrow rings and the appearance of structure; we have called it the scattering approach. The first section is devoted to describe the basic ideas behind our approach. The next section we exemplify the emergence of structured rings within scattering approach using an unrealistic toy model. We obtain non-circular narrow rings with sharp edges, that may display multiple components and arcs. Our results are qualitative so far. Yet, the approach is robust and consistent, and can be applied –with the intrinsic complications that this entails– to more realistic situations. A following section we describe the relevant phase–space structures upon which our dynamical approach is based. The last section is devoted to our conclusions and outlook.

THE SCATTERING APPROACH

Let us consider the $(N+1)$ - body full Hamiltonian which describes the motion of a central planet of mass M_0, surrounded by N_m moons and N_r ring particles ($N = N_m + N_r$). In an inertial frame we have

$$\mathcal{H} = \sum_{i=0}^{N} \frac{1}{2M_i} \left| \vec{P}_i \right|^2 - \sum_{i=1}^{N} \frac{GM_0 M_i}{\left| \vec{R}_i - \vec{R}_0 \right|} - \sum_{i>j>0}^{N} \frac{GM_i M_j}{\left| \vec{R}_i - \vec{R}_j \right|} , \qquad (1)$$

$$= \mathcal{H}_{K_m} + \mathcal{V}_{m\text{-}m} + \mathcal{H}_{K_r} + \mathcal{V}_{m\text{-}r} + \mathcal{V}_{r\text{-}r} . \qquad (2)$$

In Equation (1), $\vec{P}_i$ is the linear momentum of the i-th particle, with $i = 0$ representing the central planet, $\vec{R}_i$ is its position vector, M_i is its mass, and G is the gravitational constant. Hence, Ecuation (1) is the full many-body

problem with gravitational interactions and Equation (2) is a convenient rearrangement: $\mathscr{H}_{K_m}$ is the Hamiltonian for the keplerian two-body interaction among the moons and the planet, and $\mathscr{H}_{K_r}$ is the corresponding one among the ring particles and the central planet. The term $\mathscr{V}_{m\text{-}m}$ represents the moon-moon gravitational interaction, $\mathscr{V}_{m\text{-}r}$ is the moon-ring particle interaction and, finally, $\mathscr{V}_{r\text{-}r}$ is the ring particle–ring particle interaction. In Equation (1) we have considered purely gravitational interactions; as we shall see, our approach is quite general for conservative interactions. The assumption of purely gravitational interactions is common because the interesting structural properties observed are not related with sub-micron size (dust) particles where radiation forces and electromagnetic interactions are indeed important. For example, in Saturn's F ring, initial photometric work on Voyager's data indicated that this ring consists of a core of centimerter-size particles surrounded by micron and sub-micron material (Showalter *et al.,* 1992); later analysis on the data gathered during Saturn's ring plane crossing in 1995 suggested that the ring material is dominated by a population larger than ~10 μm with a lower cut off of 0.3–0.5 μm (Bosh *et al.*, 2002).

In the planetary case, there is a clear ordering of the masses, $M_0 \geq M_m \geq M_r$, with $M_m/M_0 \sim 10^{-8}$–10^{-4} and M_r/M_m even smaller. Here, M_m is a typical mass for the moons and M_r characterizes the mass of the ring particles. Therefore, in a first order approximation, we may neglect the contributions from $\mathscr{V}_{r\text{-}r}$, which are of second order in M_r. Physically, this amounts to ignore any effects due to ring inter-particle collisions. Moreover, due to the mass scales of the problem, the effect of individual ring particles in the motion of the planet or the moons can be neglected. This suggests to treat the motion of the individual ring particles as a restricted *n*-body problem. The motion of the central planet and the moons is solved consistently in a full many-body calculation. For the motion of the particles of the ring a solution of this many-body problem is used, which introduces an explicit time dependence. Therefore, the ring-particle Hamiltonian can be written as

$$H = \frac{1}{2}\,|\,\vec{P}\,|^2 + V_0(|\vec{X}|, t) + V_{\text{eff}}(|\vec{X}|, t) \qquad (3)$$

where V_0 refers to the dominating interaction with the central planet ($\mathscr{H}_{K_r}$), and V_{eff} is the effective interaction due to the planetary moons. The explicit time dependence in Equation (3) is related to the specific solution of the full planet–moons problem used. This is usually a kind of oscillatory motion of the moons around the central planet. Therefore, such a solution introduces an intrinsic rotation in Equation (3), which in the best case is periodic or quasi-periodic. The restricted three-body problem is an example of Equation (3), where the intrinsic rotation is precisely the circular or elliptic motion of the two-body Kepler problem between the planet and the moon.

We consider now the dynamics of the Hamiltonian Equation (3). We shall be interested in those phase–space regions that are dominated by scattering trajectories, *i.e.*, by trajectories that escape to infinity. Despite of the dominance of unbound orbits, trapping is dynamically possible. Notice that scattering trajectories define a precise physical mechanism for the particles to escape from the neighborhood of the planet–moons system, which may then create structure in the ensemble of non-escaping ring particles; hence the name of *scattering approach* (Benet and Merlo, 2004; Merlo and Benet, 2007). For simplicity we describe the case of two degrees of freedom, emphasizing that the following considerations can be generalized to more degrees of freedom.

For two degrees of freedom scattering Hamiltonian systems, the dynamics can be understood through the periodic orbits of the system, which are the organizing centers of the dynamics, and their associated invariant structures in phase–space. It is beyond the scope of this presentation to summarize the theory of chaotic scattering. Suffice it to say that, first, phase–space is the natural object to analyze the dynamics and, second, despite of the dominant role of unbounded trajectories, strictly bounded trajectories may form a set of positive measure under certain stability conditions. The latter holds because periodic orbits appear *generically* through saddle–center bifurcations. That is, as a parameter of the system is varied (*e.g.*, the Jacobi integral in the circular restricted three-body problem is reduced), two new periodic orbits appear, one is stable and the other unstable. The invariant manifolds of the unstable periodic orbit bound a region in phase–space around the stable periodic orbit, so trajectories close enough to the stable periodic orbit remain close to it for all future times. That is, test particles with initial conditions inside these phase–space regions will not escape to infinity along scattering trajectories. Further reduction of the Jacobi integral sets in a period doubling bifurcation cascade, where the elliptic point becomes inverse hyperbolic; eventually, the horseshoe structure is locally hyperbolic, which implies that the set of trapped orbits (periodic and aperiodic) is of measure zero. These results are generic for autonomous two degrees of freedom scattering Hamiltonians (Benet and Seligman, 2000; Benet, 2001); for systems with more degrees of freedom there are theorems which establish the conditions to have some *effective stability*, *i.e.*, trapped motion is proven for very long but finite times (Jorba and Villanueva, 1997a, 1997b).

In the intervals of the Jacobi integral where there is a stable periodic orbit, the manifolds of the unstable orbit define barriers which *confine dynamically* the motion of the ring particles. Such trapping actually takes place around the central planet due to the intrinsic rotation implicit in Equation (3). The trapped orbits thus remain close to the stable periodic orbit, not escaping irrespectively of whether the actual motion is periodic, quasi-periodic or even chaotic. As mentioned above, this holds generically for time-independent two degrees of freedom scattering systems; for more degrees of freedom effective dynamical trapping has been

observed (Merlo and Benet, 2007; Benet and Merlo, 2008). Generically here implies that these results only depend on the local properties of phase–space and not on the specific interaction. This makes the whole scattering approach robust in a strict mathematical sense, which physically allows to include other small conservative perturbations not included initially in Equation (1), as for instance the oblateness of the planet.

We focus on the whole interval of Jacobi integral where such dynamically trapped motion takes place. We consider an ensemble of independent ring particles, *i.e.*, non-interacting test particles, with essentially arbitrary initial conditions at $t = 0$ that belong to the specific interval where trapped motion exists. The particles whose initial conditions lie outside the region of trapped motion (for the specific value of the Jacobi integral) will rapidly escape to infinity along a scattering trajectory. In contrast, those particles within the region of trapped motion stay *dynamically* confined to trajectories close to the central periodic orbit. The distinction among these two types of initial conditions is sharp. Therefore, letting the system evolve for some time, a ring is obtained by projecting into the *X-Y* space at a given (fixed) time the phase–space location of all the ring particles of the ensemble that are dynamically confined.

From these considerations some important structural properties of the ring follow. First, the ring displays sharp edges, since the distinction between trapped particles and escaping particles is clear after rather short times. Second, the rings are in general eccentric since the motion of each particle of the ring is close to the organizing periodic orbit, which typically displays some eccentricity in a rotating frame. Third, the narrowness of the ring can be understood from the fact that the region in phase–space corresponding to dynamically bounded motion is typically very small (Benet *et al.,* 1998), as well as the interval of values of the

parameter where the reference periodic orbit is stable (Benet and Merlo 2004).

We emphasize that, despite the qualitative nature of these results, these structural properties are observed in real narrow planetary rings, and some of them are not fully understood (Esposito, 2002; Sicardy, 2005).

STRUCTURE IN NARROW RINGS USING THE SCATTERING APPROACH

In this section we review some results on the structure of the rings obtained using the scattering approach on a specific toy model. Our toy model is a planar scattering billiard on a Kepler orbit, an impenetrable disk rotating around a given point on a circular or elliptic Kepler orbit. A thorough description of the model can be found in Merlo and Benet (2007). This model is unrealistic; yet, it is the most simple realization of Equation (3), it can be studied to some extent analytically and, most important, the qualitative results obtained display consistently most –if not all– the structural properties observed in the narrow planetary rings. The rings we obtain are narrow, non-circular, sharp-edged, may display several components which are braided, and may also display non-continuous rings formed by a number of arcs. It is encouraging to note that such an unrealistic system, which only emphasizes the importance of considering scattering dynamics, can display such qualitative resemblance to the structures observed in real planetary rings. Similar results have been obtained in other systems, including the circular restricted three body problem (Merlo and Benet, 2007) and in a consistent implementation using five bodies (Olmedo, 2007) .

We begin with the scattering billiard moving on a circular orbit. In a frame rotating with the disk the new
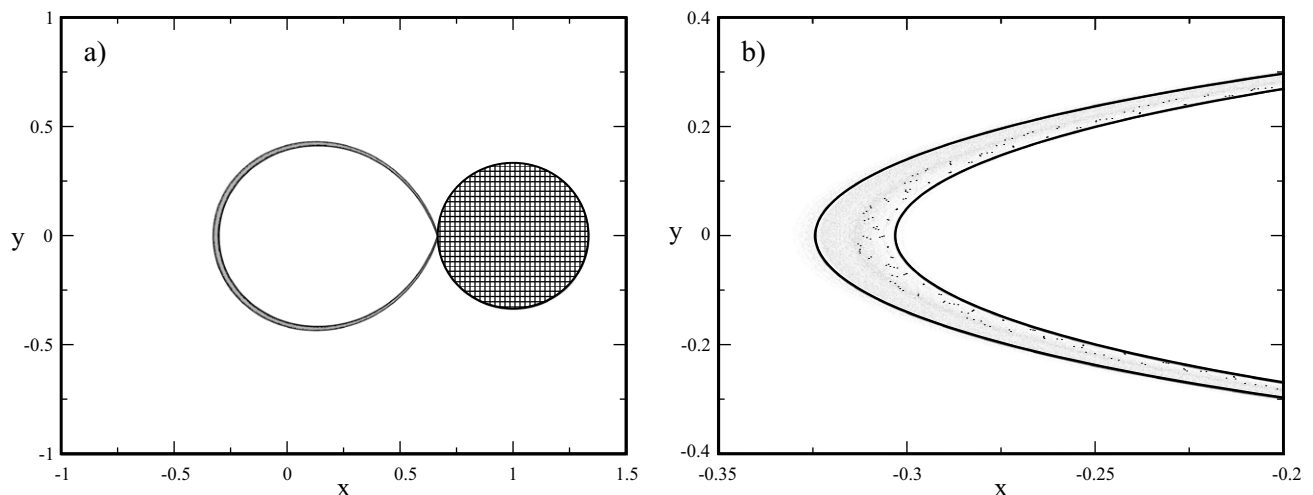
Figure 5. a) Example of a ring of non-interacting particles for the scattering billiard system on a circular orbit, in an inertial reference frame. The figure is obtained by projecting the phase space location of an ensemble of particles (inside the trapping region) onto the *X-Y* space, at a given time. b) Detail of a region of the ring. The black lines are the analytical estimates based on the stability properties of the organizing periodic orbit.

Hamiltonian becomes time independent and is therefore a conserved quantity, the Jacobi integral. In Figure 5a we plot a ring (grey region) obtained in this case; the shaded region is the hard disk; Figure 5b shows an enlargement of a region of the ring. In these figures the continuous black lines are analytical estimates given by the stability properties of the central stable periodic orbit (Benet and Merlo, 2004); as shown, they give excellent estimates of the boundaries of the ring. The ring is narrow, eccentric and does display sharp edges. In an inertial frame, the ring rotates around the origin maintaining its shape; this is due to the circular symmetry of the problem. Note that in this system the motion of each ring particle is strictly rectilinear between consecutive encounters with the disk, where it is specularly reflected in a local reference frame (Meyer *et al.,* 1995). No encounters with the disk lead to escape of the particle.

When the keplerian orbit of the disk has eccentricity $\varepsilon \neq 0$, the time dependence of the problem cannot be removed except by extending the effective number of degrees of freedom in the usual way; then, the system has more than two degrees of freedom. Figure 6a shows an enlargement of a region of the ring obtained when the disk moves on a keplerian ellipse with eccentricity $\varepsilon = 0.0001$; Figure 6b shows a detail of the ring corresponding to $\varepsilon = 0.00167$. First, we observe that the rings are narrower than the obtained one when the disk moves on a circular orbit. However, the most striking feature of the rings displayed is the fact that they are actually divided in two or more distinct components, known as strands. These strands are entangled along the azimuthal angle (measured from the contact point with the disk), forming a braided structure. The motion of the ring particles is such that, a ring particle whose initial conditions belong to a certain ring component stays in that component afterwards. In terms of the phase–space, this implies that each component belongs to an independent phase–space region; this interpretation will be confirmed
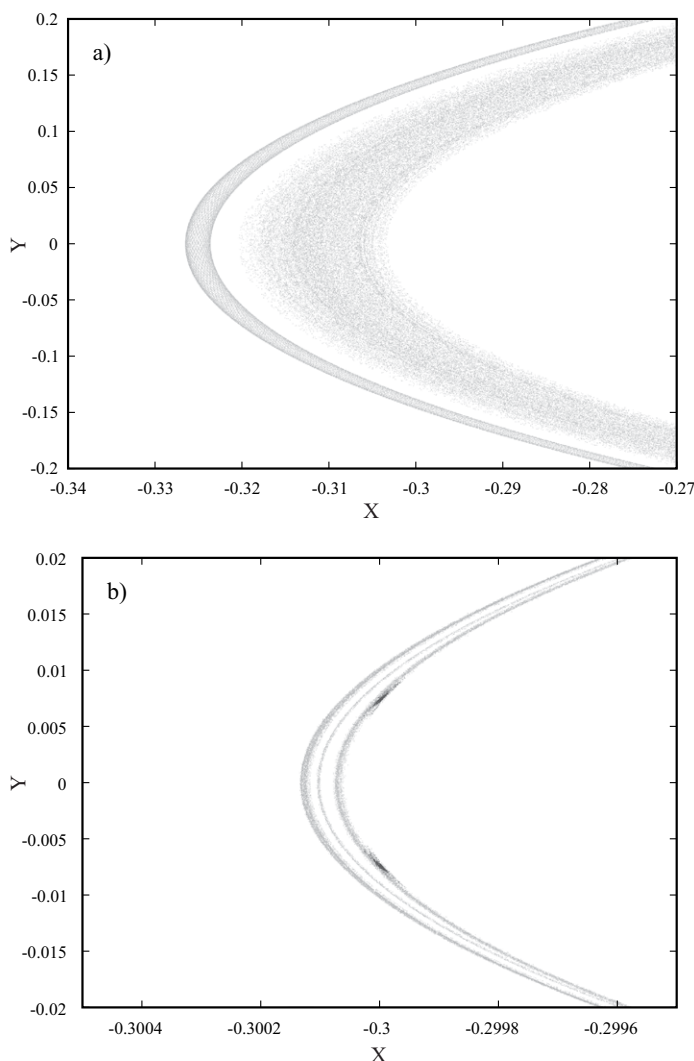
Figure 6. Detail of the ring when the disk moves on an eccentric Kepler orbit with eccentricity a) $\varepsilon = 0.0001$ and (b) $\varepsilon = 0.00167$. Note the change in the scales among the frames and with respect to Figure 1b.
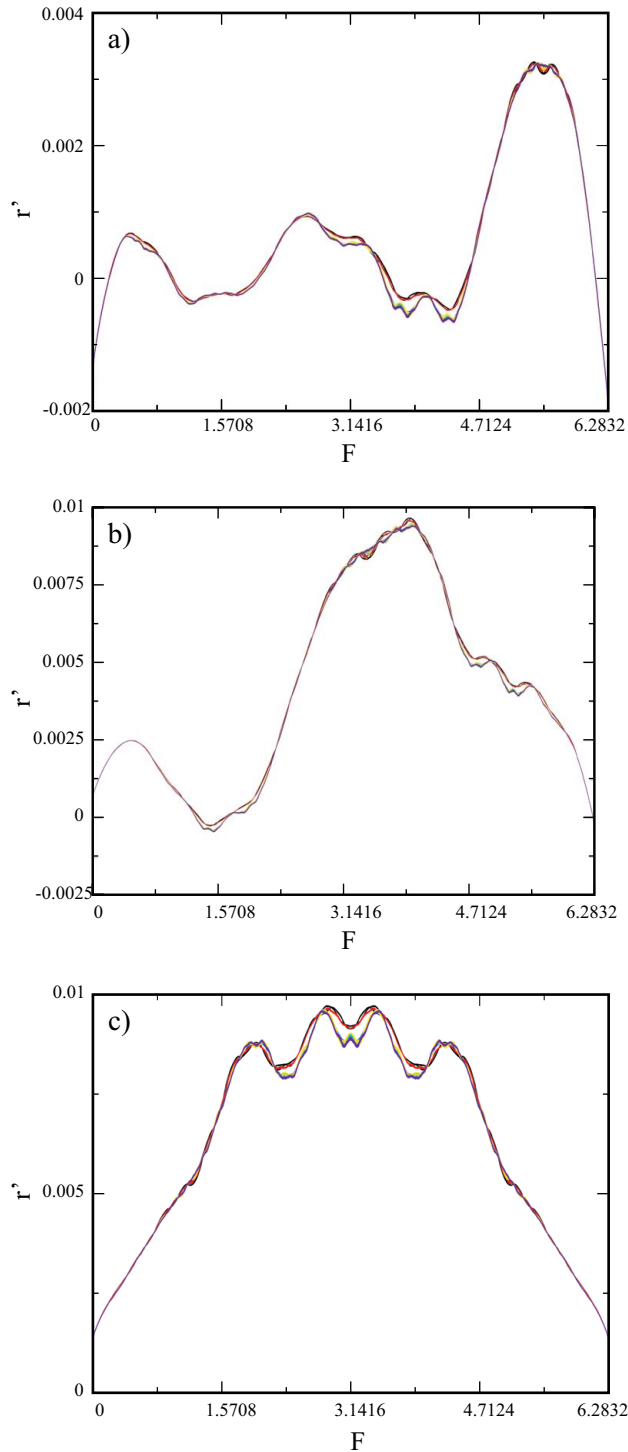
Figure 7. Whole ring represented using polar coordinates (see text), when the disk moves on an eccentric Kepler orbit with $\varepsilon = 0.00167$. Each frame represents different times t expressed as fractions of the orbital period, $T_d = 2\pi$. (a) $t = T_d/10$; (b) $t = 3T_d/10$; (c) $t = T_d/2$. Note how the different ring components entangle, forming a braided structure.

The dynamics of such multiple-component rings is rich and interesting. In Figures 7 we present the whole ring at distinct times measured as a fraction of the period of the disk, $T_d = 2\pi$, for $\varepsilon = 0.00167$. In these figures, the horizontal axis represents the polar angle measured anti-clockwise from the point in contact with the disk; the vertical axis corresponds to the radial displacement with respect to the average radial distance. First, we note in Figures 7 the clear azimuthal dependence on the radial displacement. Moreover, the figures show that each ring component, which maintains its individuality, undergoes changes in their structure independently of the others. The azimuthal dependence manifested in Figures 7 is a consequence of the broken symmetry which a non-zero eccentricity induces.

Figure 6 also manifests a subtle dependence upon the value of ε. This is further illustrated in Figure 8, where we plot the corresponding enlargement of a region of the ring obtained for $\varepsilon = 0.00168$. Comparing this figure with Figure 6b, we observe that one of the ring components, the innermost in Figure 8, has completely disappeared and a non-continuous ring has appeared. Such "patches" or arcs, are actually found everywhere in the ring. Their structure obviously recall us some clumpy behavior observed in some narrow rings in Saturn and the famous Adam's arcs in Neptune. The fact that for $\varepsilon = 0.00167$ we had three components and now there are only two and the arcs, can misleadingly be interpreted as a bifurcation which breaks one ring component in many arcs. Yet, a thorough search was carried out and our results indicate, as it was shown already in Figure 6b by the dark spots, that these arcs are indeed observed for values of ε where the third component is still present. These arcs appear from a ring componet; small changes on ε preserves them. This therefore rules out the idea that arcs follow from a bifurcation that destroys individual ring components. We finally observe that also in the ring of Figure 8 there are arcs immersed in the outermost ring component.

The above results indicate that, using the scattering approach, we indeed obtain rings which are narrow, non-circular, and have sharp edges. These properties follow naturally from the phase–space structures considered within the scattering approach, *i.e.*, the properties of the regions of trapped motion that appear literally as islands in the infinite ocean of escaping trajectories. In addition, these rings may display properties which show an azimuthal dependence: They may display multiple components which are entangled and form braids, and/or a number of localized arcs. The dynamical behavior becomes richer with new time scales which are much shorter than the period of the rotating potential. These structural properties are observed in distinct real narrow planetary rings. While all the results presented above have been illustrated using a toy model, a simple billiard system rotating on a Kepler orbit, the scattering approach is robust, and it can be applied to more realistic situations (Merlo and Benet, 2007; Olmedo, 2007).

latter. It is worth mentioning here that Saturn's F ring is precisely an example of ring with multiple components which, in addition, does not fulfill the requirements of the sheperding theory (Esposito, 2002).
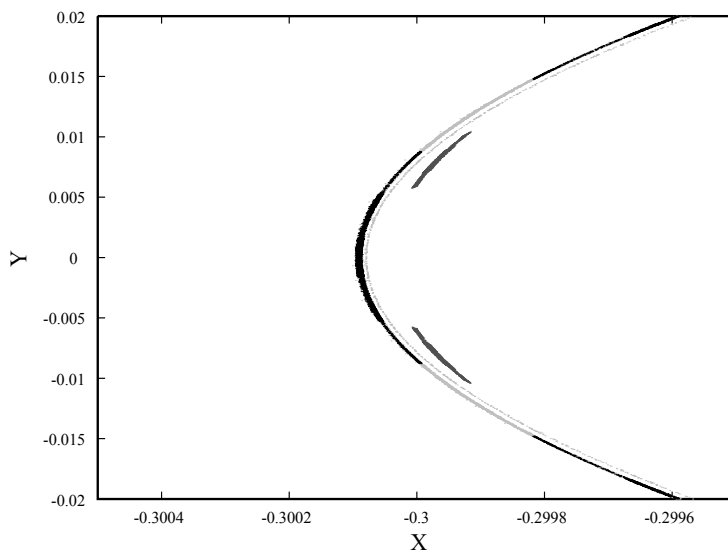
Figure 8. Detail of the ring when the disk moves on an eccentric Kepler orbit with eccentricity $\varepsilon = 0.00168$. The innermost ring component of Figure 2b has disappeared, and a discontinuous ring formed by patches or arcs is now apparent. Note that the outermost component also displays the occurrence of other set of arcs.

PHASE–SPACE CONSIDERATIONS

In this section we shall describe the phase–space structures upon which the scattering approach is based. We shall characterize the underlying changes that can take place when the Hamiltonian has more than two degrees of freedom, which are thus responsible for the appearance of multiple components and arcs.

We begin with the phase–space of a two degree of freedom Hamiltonian scattering system, with and without a region of trapped motion. As mentioned above, a *generic* scenario for the appearance of periodic orbits in Hamiltonian systems is the so called saddle–center bifurcation. Generic here implies that the same scenario holds for a large variety of interactions; the relevant aspects are the local properties. The saddle–center bifurcation occurs when, by varying a parameter of the system, two new periodic orbits are created, one of them is stable and the other unstable. In simple terms, it occurs when the solution of a quadratic equation changes from having complex roots to real-valued solutions. Just
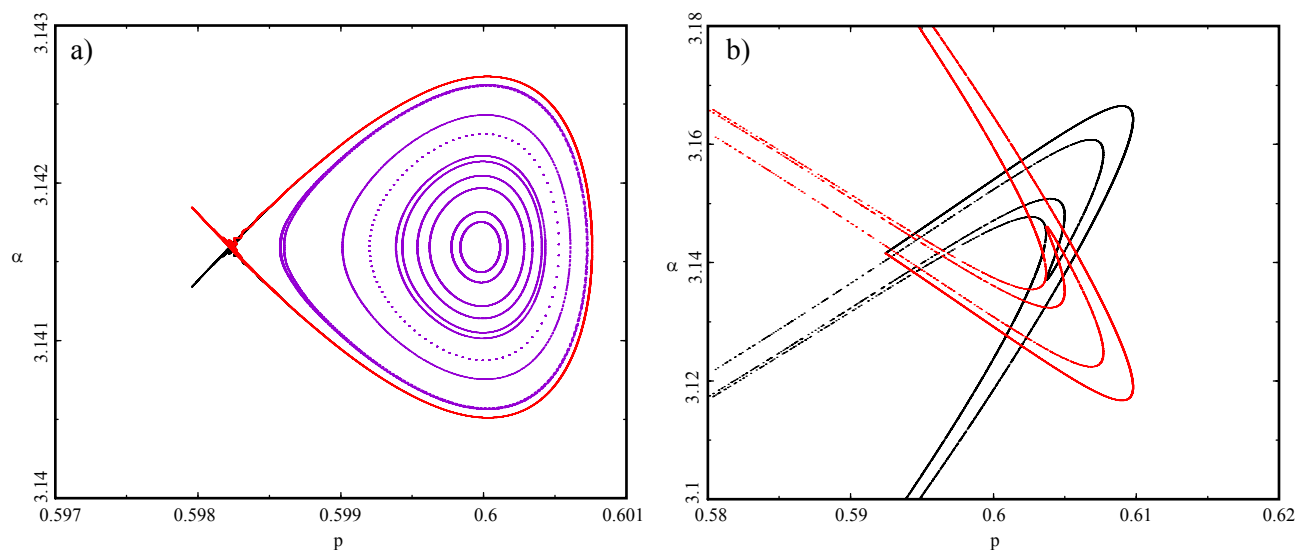
Figure 9. Poincaré surface of section displaying the structure of phase space for the scattering billiard on a circular orbit (two degree of freedom). (a) Typical structure found after the saddle–center bifurcation. The black and red curves are the manifolds of the unstable periodic orbit; they bound a region, which contains the stable periodic orbit, where trajectories cannot escape to infinity. (b) Phase-space structure when both periodic orbits are unstable. While there are orbits that never escape, the probability of finding them is zero.

after the bifurcation, the stable and unstable manifolds of the unstable periodic orbit bound a region around the stable periodic orbit (Figure 9a). Out of this region unstable motion dominates and, if the unstable fixed point is the outermost in phase–space, the corresponding (scattering) trajectories escape to infinity. On the contrary, trajectories whose initial conditions lie inside cannot escape from a vicinity of the stable fixed point and are therefore dynamically trapped. By further varying the parameter, the central stable periodic orbit typically becomes unstable through a period-doubling cascade. The phase–space changes topologically (Figure 9b), and may become eventually completely hyperbolic. For two degrees of freedom Hamiltonian systems this can be quantitatively characterized by computing the trace of the matrix that describes the linearized dynamics around a periodic orbit. When the absolute value of the trace is less than 2, the periodic orbit is stable and a region of bounded motion exists; otherwise, both periodic solutions are unstable. These elementary facts were used to construct the analytical estimates displayed in Figure 5 (see Benet and Merlo, 2004).

For more than two degrees of freedom, the topological constrains that imply that the manifolds of the unstable orbit define a bounded region around the stable one cease to apply. Arnold diffusion follows from this. This is particularly important since the explicit time dependence in Equation (3) yields an effective phase–space of five dimensions. Yet, there are theorems that provide conditions for the existence of effective bounded motion around stable tori (Jorba and Villanueva, 1997a,b). In order to obtain a graphical representation of the changes in phase–space, we shall describe the parametric behavior of a relative measure of the phase–space volume which is occupied by trapped trajectories. This, as we shall show, allows us to understand the appearance of structure in the rings.

In order to understand the appearance of the strands or arcs we need a way of characterizing the phase–space regions of trapped motion in a global way. A convenient form of achieving this, in particular when the number of degrees of freedom is more than two, is to consider the relative phase–space volume occupied by the regions of trapped motion (in the sense of effective stability) in terms of a parameter. For the scattering billiard in a circular orbit this quantity can be parameterized in terms of the Jacobi integral. Yet, the Jacobi integral is not conserved for non-zero eccentricity. We have therefore opted to use the average time between consecutive collisions with the disk, $\langle \Delta t \rangle$. Note that this quantity is equivalent to the average first-return time to a Poincaré section, which may be used in a more general context. In Figure 10 we present the structure of the relative phase–space volume for (a) $\varepsilon = 0$ and (b) $\varepsilon = 0.0001$; the corresponding rings are illustrated in Figures 5 and 6a, respectively.

In Figure 10a we observe at certain specific values of $\langle \Delta t \rangle$ that the phase–space volume of the region of trapped motion is reduced drastically. It can be shown that the

location where such abrupt reduction takes place is given by a resonant condition on the stability exponents, *i.e.*, in the (complex) phase of the eigenvalues of the linearized dynamics, and are not related to the occurrence of rational ratios among any relevant orbital periods (Benet and Merlo, 2008; Benet and Merlo, 2009); the structure of Figure 10a for two degrees of freedom Hamiltonians is universal (Contopoulos *et al.*, 1999; Contopoulos *et al.*, 2005). The structure of the histogram uncovers important aspects of the dynamics; in particular, the fine scale "jumps" mark the destruction of certain invariant curves as the parameter is changed (Simó and Vieiro, 2009). These invariant curves, if they exist bound the motion of some outlying chaotic regions; otherwise such trajectories escape along scattering trajectories. This occurs also around any secondary satellite islands, which accounts for the self-similar structure (see Simó and Vieiro, 2009).

In Figure 10b, which corresponds to $\varepsilon = 0.0001$, we observe in general some qualitative resemblance with the case $\varepsilon = 0$ (Figure 10a). However, instead of a localized drastic reduction of the phase–space volume of the trapped region as displayed in Figure 10a, in the present case a true gap is observed in the histogram. The gap appears around certain stability resonances once the eccentricity ε is non-vanishing, and is due to nonlinear effects (Benet and Merlo, 2008). Exciting such stability resonance divides the regions of trapped motion in two disjoint regions. These gaps are actually responsible for the appearance of multiple strands: If the gap is wide enough, the regions of trapped motion are, in a sense, distant in phase–space, and their projection onto the *X-Y* plane yields a ring with two independent strands. Then, the appearance of multiple-component ring follows from higher-dimensional and nonlinear effects. For a thorough description of the dependence of the histograms on $\langle \Delta t \rangle$ upon ε see Benet and Merlo (2009).

The last point we shall address here is related to the appearance of arcs. Intuitively, we expect that arcs are the result of projecting phase–space regions which resemble chains of bubbles. To understand their appearance we must mention that, *e.g.*, for $\varepsilon = 0.00167$, there are exactly 149 arcs along the whole ring. Furthermore, the exact configuration of the arcs in the *X-Y* space (labeled in an arbitrary way) is repeated after 229 bounces with the disk. These observations suggest that the appearance of arcs is linked with the mean motion resonance 149:229. Recent results confirm this, which has also served to find other occurrences of arcs (Benet and Merlo, 2009). Such resonances introduce a strong azimuthal dependence on certain trapping regions in phase–space; this seems to create, in such a higher dimensional phase–space, chains of isolated islands where trapping takes place, which seems to be an extension of the Poincaré-Birkhoff theorem for two degrees of freedom systems. We shall finally note that Adam's arcs in Neptune are understood through the occurrence of eccentricity and inclination resonances (Namouni and Porco, 2002).
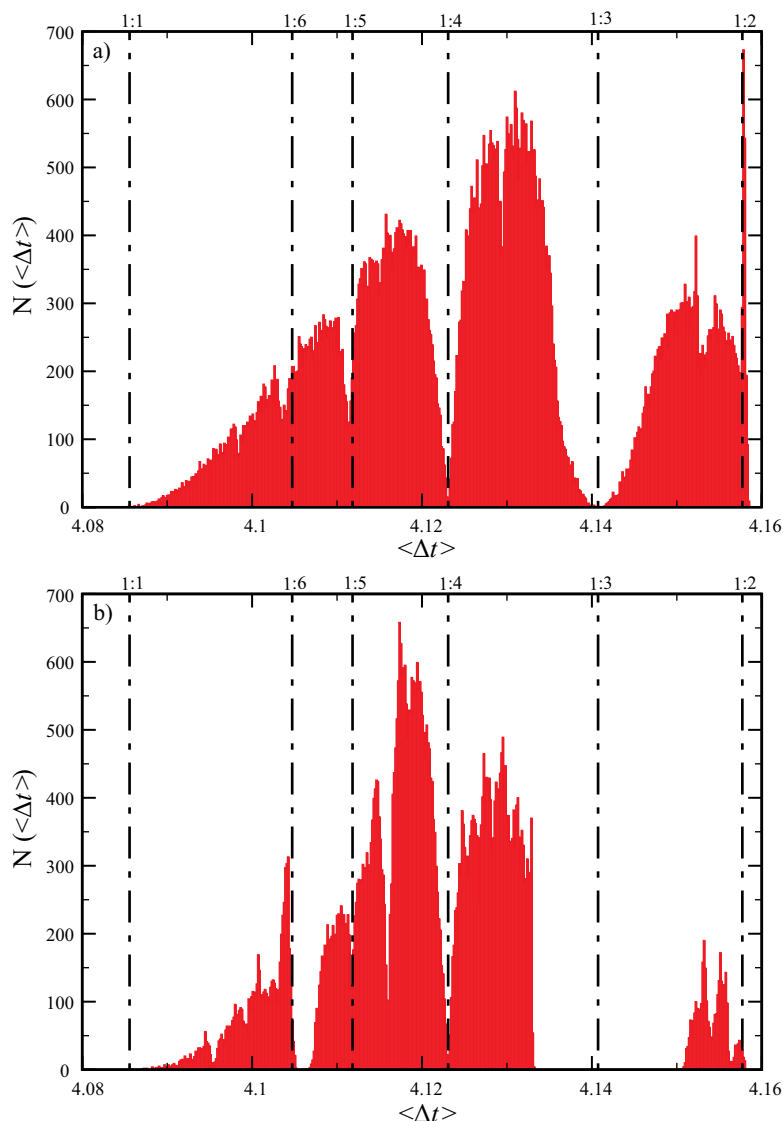
Figure 10. Histograms of the average time between consecutive collisions with the disk for an ensemble of ring particles for the scattering billiard on a Kepler orbit with (a) $\varepsilon = 0$ and, (b) $\varepsilon = 0.0001$. The histograms give a measure of the phase−space volume occupied by trapped trajectories. The main gaps are related to the stability resonances, indicated as vertical dash−dotted lines. For non−zero ε, the stability resonances separate the regions of trapped motion. This yields multiple ring components.

CONCLUSIONS AND OUTLOOK

In this paper we have reviewed some of the open problems related to the stability and structure of planetary narrow rings, and described a general and self-consistent approach to understand these issues, the scattering approach. Our approach is based on the local structure of phase–space around stable (periodic or quasi-periodic) solutions in regions where scattering dominates the dynamics. The corresponding structure in phase–space allows for a set of positive measure to exhibit dynamically trapped motion, *i.e.* a non-zero probability to find a structure resembling a ring. The basic idea is, simply, what we see is what is dynamically trapped and the structure is precisely uncovered by what it has escaped, *i.e.*, it is created by the confining mechanism.

We have illustrated our approach using an *unrealistic* toy model. Our results, which have only a qualitative value, show the occurrence of narrow non-circular rings, with sharp edges, which may display multiple components and arcs. The interest should not be the example used, but the fact that the scattering approach is robust. The results obtained in such an unrealistic system are encouraging, precisely because of the qualitative agreement with the observations. The structure that appears is understood in terms of the local properties of phase–space which is dominated by scattering trajectories. This approach can be taken over using more realistic Hamiltonian models which certainly include gravitational interactions. We are working along these lines.

ACKNOWLEDGMENTS

REFERENCES

Benet, L., 2001, Occurrence of planetary rings with shepherds: Celestial Mechanics and Dynamical Astronomy 81(1-2), 123-128.

Benet, L., Merlo, O., 2004, Phase-space structure for narrow planetary rings: Regular and Chaotic Dynamics, 9, 373-384.

Benet, L., Merlo, O., 2008, Multiple components in narrow planetary ring: Physical Review Letters, 100, 014102 (arXiv:nlin/0702039).

Benet, L., Merlo, O., 2009, Phase-Space Volume of Regions of Trapped Motion: Multiple Ring Components and Arcs: Celestial Mechanics and Dynamical Astronomy, 103(3), 209-225. (arXiv:0801.2030).

Benet, L., Seligman, T.H., 2000, Generic occurrence of rings in rotating scattering systems: Physics Letters, A273, 331-337.

Benet, L., Seligman, T. H., Trautmann, D., 1998, Chaotic Scattering in the Restricted Three-Body Problem II: Small Mass Parameters: Celestial Mechanics and Dynamical Astronomy, 71(3), 167-189.

Bosh, A.S., Olkin, C.B., French, R.G., Nicholson, P.D., 2002, Saturn's F-Ring: kinematics and particle sizes from stellar occultation studies: Icarus, 157(1), 57-75.

Borderies, N., Goldreich, P., Tremaine, S.D., 1983, The dynamics of elliptical rings: Astronomical Journal, 88, 1560-1568.

Contopoulos, G., Harsoula, M., Voglis, N., Dvorak, R., 1999, Destruction of islands of stability: Journal of Physics A: Mathematical and General 32(28), 5213-5232.

Contopoulos, G., Dvorak, R., Harsoula, M., Freistetter, F., 2005, Recurrence of order in chaos: International Journal of Bifurcations and Chaos, 15(9), 2865-2882.

Elliot, J.L., Nicholson, P.D., 1984, The rings of Uranus, *in* Greenberg, R., Brahic, A. (eds.), Planetary Rings: Tucson, Arizona, University of Arizona Press, 25-72.

Elliot, J.L., Dunham, E.W., Millis, R.L., 1977, Discovering the rings of Uranus: Sky and Telescope, 53, 412-416, 430.

Esposito, L.W., 2002, Planetary rings: Reports on Progress in Physics 65, 1741−1783.

Giuliatti-Winter, S.M., Murray, C.D., Gordon, M., 2000, Perturbations of Saturn's F-ring strands at their closest approach to Prometheus: Planetary and Space Science, 48(9), 817-827.

Goldreich, P., Tremaine, S.D., 1979, Towards a theory for the Uranian rings: Nature, 277, 97-99.

Jorba, A., Villanueva, J., 1997a, On the normal behaviour of partially elliptic lower dimensional tori of Hamiltonian systems: Nonlinearity, 10(4), 783-822.

Jorba, A., Villanueva, J., 1997b, On the persistence of lower dimensional invariant tori under quasi-periodic perturbations: Journal of Nonlinear Science, 7(5), 427-473.

Hänninen, J., 1993, Numerical simulation of moon−ringlet interactions: Icarus, 103(1), 104-123.

Lewis, M.C., Stewart, G.R., 2000, Collisional dynamics of perturbed planetary rings: The Astronomical Journal, 120, 3295-3310.

Lissauer, J.J., Peale, S.J., 1986, The production of "braids" in Saturn's F ring: Icarus, 67(3), 358-374.

Merlo, O., Benet, L., 2007, Strands and braids in narrow planetary rings: A scattering system approach: Celestial Mechanics and Dynamical Astronomy, 97(1), 49-72.

Meyer, N., Benet, L., Lipp, C., Trautmann, D., Jung, C., Seligman, T.H., 1995, Chaotic scattering off a rotating target: Journal of Physics A: Mathematical and General 28, 2529-2544.

Murray, C.D., Dermott, S.F., 1999, Solar System Dynamics: Cambridge, Cambridge University Press, 612 pp.

Murray, C.D., Thompson, R.P., 1990, Orbits of shepherd satellites deduced from the structure of the rings of Uranus: Nature, 348, 499-502.

Murray, C.D., Gordon, M.K., Giuliatti-Winter, S.M., 1997, Unraveling the Strands of Saturn's F Ring: Icarus, 129(2), 304-316.

Murray, C.D., Chavez, C., Beurle, K., Cooper, N., Evans, M.W., Burns, J.A., Porco,C.C., 2005, How Prometheus creates structure in Saturn's F ring: Nature 437, 1326-1329.

Namouni, F., Porco, C., 2002, The confinement of Neptune's ring arcs by the moon Galatea: Nature, 417, 45-47.

Olmedo-Casal, E., 2007, On the parallel computation of invariant tori: Barcelona, Universitat de Barcelona, PhD thesis.

Ogilvie, G.I., 2007, Mean-motion resonances in satellite-disc interactions: Monthly Notices of the Royal Astronomical Society, 374(1), 131-149.

Showalter, M.R., Burns, J.A., 1982, A numerical study of Saturn's F ring: Icarus, 52(3), 526-544.

Showalter, M.R., Pollack, J.B., Ockert, M.E., Doyle, L.R., Dalton, J.B., 1992, A photometric study of Saturn's F-Ring: Icarus, 100(2), 394-411.

Sicardy, B., 2005, Dynamics and Composition of Rings: Space Science Reviews, 116(1-2), 457-470.

Smith, B.A., Soderblom, L., Beebe, R., Boyce, J., Briggs, G., Bunker, A., Collins, S.A., Hansen, C.J., Johnson, T., Mitchell, J.L., Terrile, R.J., Carr, M., Cook II, F.A., Cuzzi, J., Pollack, J.B., Danielson, G., Ingersoll, A., Davies, M.E., Hunt, G.E., Masursky, H., Shoemaker, E., Morrison, D., Owen, T., Sagan, C., Veverka, J., Strom, R., Suomi, V.E., 1981, Encounter with Saturn: Voyager 1 imaging science results: Science, 212(4491), 163-191.

Smith, B.A., Soderblom, L., Batson, R., Bridges, P., Inge, J., Masursky, H., Shoemaker, E., Beebe, R., Boyce, J., Briggs, G., Bunker, A., Collins, S.A., Hansen, C.J., Johnson, T.V., Mitchell, J.L., Terrile, R.J., Cook II, A.F., Cuzzi, J., Pollack, J.B., Danielson, E., Ingersoll, A.P., Davies, M.E., Hunt, G.E., Morrison, D., Owen, T., Sagan, C., Veverka, J., Strom, R., Suomi, V.E., 1982, A new look at the Saturn system: The Voyager 2 images: Science, 215(4532), 504-537.

Simó C., Vieiro A., 2009, Resonant zones, inner and outer splittings in generic and low order resonances of area preserving maps: Nonlinearity, 22(5), 1191-1245.